Finite element dynamical subgrid-scale model for low Mach number flows with radiative heat transfer

Received 31 July 2014
Revised 26 October 2014
Accepted 11 December 2014

Matias Avila
Barcelona SuperComputing Center, Barcelona, Spain
R. Codina
Universitat Politècnica de Catalunya, Barcelona, Spain, and
Javier Principe
International Center of Numerical Methods in Engineering (CIMNE), Universitat Politècnica de Catalunya, Barcelona, Spain

Abstract

Purpose – The purpose of this paper is to present a finite element approximation of the low Mach number equations coupled with radiative equations to account for radiative heat transfer. For high-temperature flows this coupling can have strong effects on the temperature and velocity fields.

Design/methodology/approach – The basic numerical formulation has been proposed in previous works. It is based on the variational multiscale (VMS) concept in which the unknowns of the problem are divided into resolved and subgrid parts which are modeled to consider their effect into the former. The aim of the present paper is to extend this modeling to the case in which the low Mach number equations are coupled with radiation, also introducing the concept of subgrid scales for the radiation equations.

Findings – As in the non-radiative case, an important improvement in the accuracy of the numerical scheme is observed when the nonlinear effects of the subgrid scales are taken into account. Besides it is possible to show global conservation of thermal energy.

Originality/value – The original contribution of the work is the proposal of keeping the VMS splitting into the nonlinear coupling between the low Mach number and the radiative transport equations, its numerical evaluation and the description of its properties.

Keywords Finite element analysis, Radiative heat transfer, Stabilization, Thermal flows, Variational multiscale

Paper type Research paper

1. Introduction

Thermal radiation in gas flows has direct effects on many industrial applications, such as fires, furnaces, gas turbines, boilers, etc., where radiative transfer dominates heat transfer. Growing concern with high-temperature flows has emphasized the need for an evaluation of the effect of radiative heat transfer. Radiation can strongly interact with convection in many situations of engineering interest and neglecting its effects may have significant consequences in the overall predictions. An accurate calculation of

The authors acknowledge the financial support received from the Spanish Ministry of Economics and Competitiveness, National Programme of R&D to the project PARANAT (ENE2011-28825). R. Codina also acknowledges the financial support received from the ICREA Acadèmia Program, from the Catalan Government.

International Journal of Numerical Methods for Heat & Fluid Flow
Vol. 25 No. 6, 2015
pp. 1361-1384

0961-5539
DOI 10.1108/HFF-07-2014-0238

radiative transfer is then of crucial importance for the prediction of the thermal performance. Nevertheless, it is common for studies on convective flows to neglect thermal radiation, mainly because the modeling of radiative transfer increases the computational work and involves tedious analytical developments. A notable exception is Dubroca *et al.*, (2007).

Approximate models for radiative heat transfer have been derived and widely used in the literature. Examples of such approximation are the P_N method (Davison, 1958, Modest, 1976) and the discrete ordinates method (DOM) (Truelove, 1987; Modest, 1976). Our interest in this work is the development of a nonlinear stabilization technique capable of solving low Mach number flows in radiating media without being focussed in a specific radiative model.

Turbulence is the most common state of a fluid in a wide range of technologies and natural conditions. The interaction between turbulence and radiation (TRI) has been demonstrated experimentally, theoretically and numerically, and results from the highly nonlinear coupling between fluctuations of radiation intensity and fluctuations of temperature of the medium (Coelho, 2007). Experimental data and numerical calculations demonstrate that turbulent fluctuations may significantly increase the radiation intensity in both non-luminous and luminous flames. The net radiative power and the fraction of radiative heat loss increase due to TRI. Usually, in combustion applications using large eddy simulation (LES), these interactions are either discarded altogether, or included in the computation without considering any subgrid-scale model for radiation.

The focus of the present paper is on how to compute the coupling of the radiative terms in the energy equation and the thermal terms in the radiative equations. In this work we extend the stabilized finite element approximation presented in Avila *et al.* (2011a, b), valid for low Mach number flows, for the presence of radiative heat transfer. The stabilization method is based on the variational multiscale (VMS) method (Hughes, 1995), in which a decomposition of the approximating space into a coarse scale resolvable part and a fine scale subgrid part is performed. The distinctive features of our particular approach, discussed in Avila *et al.* (2011a, b), are to consider the subgrid scales as transient and to keep the scale splitting in all the nonlinear terms. The first ingredient permits to obtain better stability and no restrictions on the time step size. The second ingredient permits to prove global conservation properties, gives higher accuracy to the method and allows us to approach the problem of dealing with thermal turbulence from a strictly numerical point of view, as it was shown in Avila *et al.* (2014). The improvements of the formulation when using the nonlinear VMS method (Avila *et al.* 2011a, b, 2014) in respect to classical stabilization methods such as SUPG are due to the nonlinear nature of the low Mach number equations. The potential of the present stabilization method to model all kinds of turbulent thermally coupled flows without using any turbulence closure or physical model was demonstrated in Avila *et al.* (2014). In Avila *et al.* (2011a, b) the radiation transport equation (RTE) was discretized in space using the VMS stabilization method, comparing the stability properties and the accuracy of the obtained results against the classical SUPG method and the Galerkin method. However, the obtained results did not show an important improvements of the VMS method with respect to the SUPG method, showing both methods a similar behavior. The reason for this is because the RTE is a linear equation, and the VMS method we propose yields improvements when applied to nonlinear equations.

There have been some significant works on finite element method (FEM) solving the RTE, using different stabilization techniques. Razzaque *et al.* (1983) studied the finite element solution of radiative heat transfer in a twodimensional (2D) rectangular enclosure.

Zhao and Liu (2007) discretized using FEM a derived second-order, diffusion-type, radiative equation. An *et al.* (2005) developed a finite element formulation for the RTE using triangular isoparametric finite elements. In the present work we extend the formulation presented in Avila *et al.* (2011a, b, 2014) to radiative flows without focussing in any specific radiative model. The aim of the present work is to show that the nonlinear stabilization terms coming from the highly nonlinear coupling between temperature and radiation ($\kappa\sigma_B T^4$, see below for the notation) are able to model TRI subgrid effect.

The paper is organized as follows. In Section 2, the low Mach number equations with radiative coupling and their variational formulation are given. Some different coupling mechanisms between radiative and conductive heat transfer are presented. Afterwards the VMS formulation with dynamic scale splitting is derived in Section 3. Section 4 is devoted to show that this formulation provides global energy conservation when using equal interpolation spaces for pressure and temperature, if the radiation model is globally conservative. The treatment of the coupling of the nonlinear terms is described in detail in Section 5. The formulation is tested in Section 6 and conclusions are drawn in Section 7.

2. The low Mach number problem coupled with radiative heat transfer

2.1 Initial and boundary value problem

Our interest is directed to low speed strongly thermally coupled flows which are described by the compressible Navier-Stokes equations in the low Mach number limit. This limit is derived by an asymptotic expansion of the problem variables as power series of the small parameter $\mathrm{Ma}^2 \ll 1$, where Ma denotes the Mach number of the problem. As a particular result of this process, the total pressure is split into two parts, the thermodynamic part $p^{\mathrm{th}}(t)$ which is uniform in space, and the hydrodynamic part $p(x, t)$ which is several orders of magnitude smaller than p^{th} and is therefore omitted in the state and energy equations. This leads to a removal of the acoustic modes but large variations of density due to temperature variations are allowed. A detailed analysis for the standard Ma^2 expansion and many aspects of low Mach number asymptotics can be found in Zeytounian (2010). The low-Mach-number flow equations and the finite element approximation we propose for them were introduced in Avila *et al.* (2011a, b). When radiative heat transfer is considered the energy equation is modified by adding the divergence of the total radiative heat flux term, $\nabla \cdot \boldsymbol{q}_r$. The initial and boundary value problem reads as follows. Let $\Omega \subset \mathbb{R}^d$, with $d = 2, 3$, be the computational domain in which the flow takes place during the time interval $[0, t_{\mathrm{end}}]$, and let $\partial\Omega$ be its boundary. Let $\mathcal{S}^2$ be the unit sphere in $\mathbb{R}^3$. The initial and boundary value problem to be considered consists in finding a velocity field $\boldsymbol{u}$, a hydrodynamic pressure field p, a temperature field T, the thermodynamic pressure p^{th} and the radiation intensity field I_λ such that:

$$\frac{\partial \rho}{\partial t} + \nabla \cdot (\rho \boldsymbol{u}) = 0 \quad \text{in } \Omega, t \in (0, t_{\mathrm{end}}) \tag{1}$$

$$\rho \frac{\partial \boldsymbol{u}}{\partial t} + \rho \boldsymbol{u} \cdot \nabla \boldsymbol{u} - \nabla \cdot (2\mu\varepsilon'(\boldsymbol{u})) + \nabla p = \rho \boldsymbol{g} \quad \text{in } \Omega, t \in (0, t_{\mathrm{end}}) \tag{2}$$

$$\rho c_p \frac{\partial T}{\partial t} + \rho c_p \boldsymbol{u} \cdot \nabla T - \nabla \cdot (k \nabla T) + \nabla \cdot \boldsymbol{q}_r - \frac{\mathrm{d}p^{\mathrm{th}}}{\mathrm{d}t} = Q \quad \text{in } \Omega, t \in (0, t_{\mathrm{end}}) \tag{3}$$

$$\boldsymbol{s} \cdot \nabla I_\lambda + (\kappa_\lambda + \sigma_{s\lambda}) I_\lambda - \frac{\sigma_{s\lambda}}{4\pi} \int_{\mathcal{S}^2} \mathrm{d}s' \phi_\lambda(s', s) I_\lambda(s') = \kappa_\lambda I_{b\lambda} \quad \text{in } \Omega \times \mathcal{S}^2, t \in (0, t_{\mathrm{end}}) \tag{4}$$

where ρ denotes the density, μ the viscosity, $\varepsilon'(\boldsymbol{u}) = \varepsilon(\boldsymbol{u}) - (1/3)(\nabla \cdot \boldsymbol{u})\boldsymbol{I}$ the deviatoric part of the rate of deformation tensor $\varepsilon(\boldsymbol{u}) = \nabla^s \boldsymbol{u} = 1/2\left(\nabla \boldsymbol{u} + \nabla \boldsymbol{u}^T\right)$, $\boldsymbol{I}$ the identity tensor, $\boldsymbol{g}$ the gravity acceleration vector, c_p the specific heat coefficient at constant pressure, k the thermal conductivity and Q the heat source. Equations (1)-(3) represent the mass, momentum and energy conservation, respectively. Equation (4) is the monochromatic radiative transfer equation, and $I_\lambda(s)$ is the spectral radiative intensity at wavelength λ propagating in direction s. The function $I_{b\lambda}$ is the spectral blackbody radiation at wavelength λ, depending only on the temperature T. The coefficients k_λ and $\sigma_{s\lambda}$ are respectively the spectral absorption and scattering coefficients, $\phi_\lambda(\boldsymbol{s}', \boldsymbol{s})$ is the scattering phase function and $\mathrm{d}s'$ the differential of solid angle. The total time derivative operator $\mathrm{d}/\mathrm{d}t$ was used over p^{th}, because this variable only depends on time. The inverse of the light-speed has been considered negligible when writing Equation (4). This is a valid approximation for the vast majority of engineering applications, where the speed of light is much larger than the ratio between the time and length scales of the problem. Therefore, the radiative heat transfer can be consider as steady state (or propagating at infinite velocity). Additionally, the state equation for ideal gases is used to give a closure to the system:

$$\rho = p^{\mathrm{th}}/RT \tag{5}$$

The radiative heat transfer term in the energy equation, which is the one coupling both problems (also through the boundary conditions, see below), can be expressed in terms of radiative intensity and temperature as:

$$\nabla \cdot \boldsymbol{q}_r = \int_0^\infty \mathrm{d}\lambda \kappa_\lambda (4\pi I_{b\lambda} - G_\lambda) = 4\kappa_e \sigma_B T^4 - \kappa_a G(I_\lambda) \tag{6}$$

where G_λ and G are the spectral and total incident radiation, defined as:

$$G_\lambda = \int_{S^2} \mathrm{d}s I_\lambda \tag{7}$$

$$G(I_\lambda) = \int_0^\infty \mathrm{d}\lambda G_\lambda. \tag{8}$$

The absorption and emission coefficients k_a and k_e in Equation (6) are spectral averages of the absorption coefficient k_λ, weighted respectively with the radiation field G_λ and the blackbody radiation field $I_{b\lambda}$:

$$\kappa_a = \frac{\int_0^\infty \mathrm{d}\lambda \kappa_\lambda G_\lambda}{G} \tag{9}$$

$$\kappa_e = \frac{\pi \int_0^\infty \mathrm{d}\lambda \kappa_\lambda I_{b_\lambda}}{\sigma_B T^4} \tag{10}$$

where σ_B is the Stephan-Boltzmann constant. For a given composition and pressure, the emissivity coefficient only depends on temperature.

The mass, momentum and energy equations must be supplied with initial and boundary conditions. Initial conditions are:

$$\boldsymbol{u} = \boldsymbol{u}_0 \quad \text{in } \Omega, t = 0$$

$$T = T_0 \quad \text{in } \Omega, t = 0$$

$$p^{\text{th}} = p_0^{\text{th}} \quad \text{in } \Omega, t = 0$$

Dirichlet and Neumann boundary conditions for Equations (1) and (3) are:

$$\boldsymbol{u} = 0 \quad \text{in } \Gamma_D^{\boldsymbol{u}} \tag{11}$$

$$T = 0 \quad \text{in } \Gamma_D^T \tag{12}$$

$$(-p\boldsymbol{I} + 2\mu\varepsilon'(\boldsymbol{u})) \cdot \boldsymbol{n} = \boldsymbol{t}_n \text{ in } \Gamma_N^{\boldsymbol{u}} \tag{13}$$

$$-k\boldsymbol{n} \cdot \nabla T = q_n \quad \text{in } \Gamma_N^T \tag{14}$$

where $\boldsymbol{n}$ is the unit normal vector on the boundary pointing outwards the domain. It is assumed that $\Gamma_D^x \cup \Gamma_N^x = \partial\Omega$, and $\Gamma_D^x \cap \Gamma_N^x = \emptyset$ for $x = T$, $\boldsymbol{u}$.

Due to the hyperbolic nature of the radiation Equation (4), the intensity entering into the domain Ω needs to be imposed. The boundary $\Gamma = \partial\Omega \times \mathcal{S}^2$ of $\Omega \times \mathcal{S}^2$ is divided into the inflow Γ^- and outflow Γ^+ boundaries, defined as:

$$\Gamma^- = \{(\boldsymbol{x}, \boldsymbol{s}) \in \Gamma | \boldsymbol{s} \cdot \boldsymbol{n} < 0\}, \quad \Gamma^+ = \{(\boldsymbol{x}, \boldsymbol{s}) \in \Gamma | \boldsymbol{s} \cdot \boldsymbol{n} \geqslant 0\},$$

we shall also make use of the inflow and outflow hemispheres

$$S_{\boldsymbol{x}}^- := \left\{ s \in S^2 \middle| \boldsymbol{s} \cdot \boldsymbol{n} < 0 \right\}, \quad S_{\boldsymbol{x}}^+ := \left(\boldsymbol{s} \in S^2 \middle| \boldsymbol{s} \cdot \boldsymbol{n} \geqslant 0 \right),$$

which are defined for each $\boldsymbol{x} \in \partial\Omega$.

The radiative transfer Equation (4) is subject to emissive and reflective boundary conditions of the form:

$$I_\lambda(\boldsymbol{x}, \boldsymbol{s})\big|_{S_{\boldsymbol{x}}^-} = \varepsilon_\lambda I_{b\lambda} + \frac{r_\lambda}{\pi} \int_{\boldsymbol{S}_{\boldsymbol{x}}^+} I_\lambda(\boldsymbol{x}, \boldsymbol{s}) \boldsymbol{n} \cdot \boldsymbol{s} \, \mathrm{d}s \tag{15}$$

where ε_λ and r_λ are, respectively, the emission and reflective wall coefficients at wavelength λ. In the present work we consider opaque surfaces, where $r_\lambda = 1 - \varepsilon_\lambda$.

In some applications the Neumann boundary condition defined by Equation (14) is changed to impose the complete heat transfer (conductive and radiative) $\mathcal{H}$ through the boundary as:

$$-k\boldsymbol{n} \cdot \nabla T + \boldsymbol{q}_r \cdot \boldsymbol{n} = \mathcal{H} \tag{16}$$

An example is a boundary where the net flux through the boundary is null ($\mathcal{H}=0$). This wall is an emmisive and reflective wall, i.e. the radiation boundary condition Equation (15) is satisfied. The radiative heat flux through the boundary is:

$$\boldsymbol{q}_r \cdot \boldsymbol{n} = \int_\lambda d\lambda \int_S \mathrm{d}s I_\lambda(\boldsymbol{x}, \boldsymbol{s}) \boldsymbol{s} \cdot \boldsymbol{n} \tag{17}$$

Integrating boundary condition Equation (15) over S_x^- and λ permits to obtain:

$$\boldsymbol{q}_r \cdot \boldsymbol{n} = (1-r)H - \varepsilon \sigma_B T^4 \tag{18}$$

$$-k\boldsymbol{n} \cdot \nabla T - \varepsilon \sigma_B T^4 = \mathcal{H} - (1-r)H \tag{19}$$

where $H(\boldsymbol{x})$ is the surface irradiation:

$$H(\boldsymbol{x}) = \int_\lambda d\lambda \int_{\boldsymbol{S}_x^+} ds I_\lambda(\boldsymbol{x}, \boldsymbol{s}) \boldsymbol{s} \cdot \boldsymbol{n} \tag{20}$$

and r is the spectral average of r_λ weighted with the irradiation and ε is the spectral average of ε_λ weighted with the blackbody radiation $I_{b\lambda}$. This boundary condition is of nonlinear Robin type for the temperature, coupling radiation and temperature in the boundary.

The coupling between the radiation and the hydrodynamic problems is stronger on the boundaries than inside the media when the medium is optically thin. This occurs when the characteristic length of the problem (L_0) is much smaller than the optical length scale (κ_0^{-1}), and it is characterized by a small optical length number $\tau = k_0 L_0 \ll 1$. On the other hand, when the medium is optically thick it is usual to take $L_0 = 1/k_e$ (i.e. $\tau = 1$) and in this case the coupling between both problems occurs locally inside the domain. In this case the relative importance of radiative heat and conductive heat transfer is estimated by the Planck number, $\mathrm{Pl} = k\kappa_e/\sigma_B T_0^3$, also known as the radiation to conduction parameter (Modest, 2003).

2.2 Directional discretization

Whereas the hydrodynamic equations problem defined Equations (1)-(3) is 3D, the radiative transfer Equation (4) is higher dimensional: the radiation intensity depends on six independent variables (three space coordinates, two direction coordinates and the wavelength). Therefore its discretization, which is usually very expensive, requires the introduction of basis functions in $\mathcal{S}^2$ and in the (1D) wavenumber space. There exist several models to obtain an approximate solution to the radiation transfer equation. An usual option is to apply a directional discretization, transforming the integro-differential Equation (4) into a set of coupled differential equations, with an arbitrary number of equations depending on the discretization level. Examples of this kind of models are the DOM, the method of spherical harmonics (P_N-approximation) and the ray tracing method. The resulting equations can then be discretized in space using the FEM, as for example in Hun-Kang and Song (2008).

The aim of the present paper is to develop a stabilization method for the mass, momentum and energy equations, independent of the radiative model used. We therefore assume that a general directional discretization model is applied to the radiative transfer equation, obtaining directional components of radiation intensity I_λ^d.

The radiation equation of the adopted model will be denoted as $\mathcal{R}_M\left(I_\lambda^d, T\right)=0$, where $\mathcal{R}_M$ is a partial differential operator and I_λ^d the semidiscrete radiation intensity. In the energy equation, the emission coefficient k_e and the product of the absorption coefficient and the incident radiation k_aG will depend on the obtained radiation intensity distribution I_λ^d, and must be given by the radiative model.

2.3 Variational formulation

To obtain a variational formulation for the system Equations (1)-(3) together with the radiation model equation, let us denote by $\boldsymbol{V}$, Q, W, Z the functional spaces where the solution is sought. The corresponding space of test functions will be denoted by $\boldsymbol{V}_0$, Q_0, W_0, Z_0.

The weak form of the problem consists in finding $\left(\boldsymbol{u}, p, T, I_\lambda^d\right) \in (\boldsymbol{V} \times Q \times W \times Z)$ such that:

$$\left(\frac{\partial \rho}{\partial t}+\nabla\cdot(\rho \boldsymbol{u}), q\right)=0 \quad \forall q \in Q_0 \tag{21}$$

$$\begin{aligned}&\left(\rho\tfrac{\partial u}{\partial t}+\rho \boldsymbol{u}\cdot\nabla \boldsymbol{u}, \boldsymbol{v}\right)+(2\mu\varepsilon'(\boldsymbol{u}), \varepsilon'(v))\\ &\quad -(p, \nabla\cdot \boldsymbol{v})=(\rho \boldsymbol{g}, v)+(\boldsymbol{t}_n, \boldsymbol{v})_{\Gamma_N^u} \quad \forall \boldsymbol{v} \in \boldsymbol{V}_0\end{aligned} \tag{22}$$

$$\begin{aligned}&\left(\rho c_p\tfrac{\partial T}{\partial t}+\rho c_p \boldsymbol{u}\cdot\nabla T+\kappa_e\sigma_B T^4, w\right)+(k\nabla T, \nabla w)\\ &\quad=\left(Q+\tfrac{\mathrm{d}p^{\mathrm{th}}}{\mathrm{d}t}+\kappa_a G(I_\lambda), w\right)+(q_n, w)_{\Gamma_N^T} \quad \forall w \in W_0\end{aligned} \tag{23}$$

$$\left(\mathcal{R}_M\left(I_\lambda^d, T\right), z\right)=0 \quad \forall z \in Z_0 \tag{24}$$

where $(\cdot, \cdot)$ denotes the $L^2\Omega$ inner product of two functions, either scalars or vectors.

3. Spatial approximation of the coupled radiation and low Mach number equations

Let us consider a finite element partition $\{K\}$ with n_e elements of the computational domain Ω, from which we can construct finite element spaces for the velocity, pressure, temperature and radiation intensity in the usual manner. We will denote them by $\boldsymbol{V}_h \subset \boldsymbol{V}$, $Q_h \subset Q$, $W_h \subset W$ and $Z_h \subset Z$, respectively.

Let us split the continuous space $\boldsymbol{Y}=\boldsymbol{V} \times Q \times W \times Z$ where velocity, pressure, temperature and radiation intensity belong, as $\boldsymbol{Y}=\boldsymbol{Y}_h \oplus \tilde{\boldsymbol{Y}}$, where $\tilde{\boldsymbol{Y}}=\tilde{\boldsymbol{V}} \times \tilde{Q} \times \tilde{W} \times \tilde{Z}$ is the subgrid space, that can be in principle any space to complete $\boldsymbol{Y}_h=\boldsymbol{V}_h \times Q_h \times W_h \times Z_h$ in $\boldsymbol{Y}$. These continuous unknowns split as:

$$\boldsymbol{u}=\boldsymbol{u}_h+\tilde{\boldsymbol{u}} \tag{25}$$

$$p=p_h+\tilde{p} \tag{26}$$

$$T=T_h+\tilde{T} \tag{27}$$

$$I_{\lambda h}^d=I_{\lambda h}^d+\tilde{I_\lambda^d} \tag{28}$$

where the components with subscripts h belong to the corresponding finite element spaces, and the components with the ~ correspond to the subgrid space. These additional components are what we will call subgrid scales.

The spatial approximation will be obtained following the same procedures and approximations done in Avila *et al.* (2011a, b) for the low Mach number equations. The particular approximation consists in keeping time dependency of the subgrid scales and to keep the previous decompositions Equations (25)-(27) in all the terms of the variational problem Equations (21)-(24) even if the differential operator is approximated. It is assumed that the subgrid scales vanish on the interelement boundaries, ∂K.

Substituting decompositions Equations (25)-(27) in the variational problem Equations (21)-(23), taking the tests functions in the corresponding finite element spaces and integrating some terms by parts, it is found that the solution $\left(\boldsymbol{u}_h, T_h, p_h, I^d_{\lambda h}\right) \in \boldsymbol{V}_h \times Q_h \times W_h \times Z_h$ must satisfy:

$$\left(\frac{\partial \rho^h}{\partial t}, q_h\right) - \left(\rho^h \boldsymbol{u}_h, \nabla q_h\right) + \left(\rho^h \boldsymbol{n} \cdot \boldsymbol{u}_h, q_h\right)_{\partial\Omega} - \left(\rho^h \tilde{\boldsymbol{u}}, \nabla q_h\right) = 0 \tag{29}$$

$$\begin{aligned} &\left(\rho^h \tfrac{\partial \boldsymbol{u}_h}{\partial t} + \rho^h (\boldsymbol{u}_h + \tilde{\boldsymbol{u}}) \cdot \nabla \boldsymbol{u}_h, \boldsymbol{v}_h\right) + \left(2\mu\varepsilon'(\boldsymbol{u}_h), \nabla^s \boldsymbol{v}_h\right) - \left(p_h, \nabla \cdot \boldsymbol{v}_h\right) \\ &\quad - \left(\tilde{\boldsymbol{u}}, -\tfrac{\partial \rho^h}{\partial t} \boldsymbol{v}_h + \rho^h (\boldsymbol{u}_h + \tilde{\boldsymbol{u}}) \cdot \nabla v_h + \nabla^h \cdot (2\mu\varepsilon(\boldsymbol{v}_h))\right) \\ &\quad + \left(\tfrac{\partial (\rho^h \tilde{\boldsymbol{u}})}{\partial t}, \boldsymbol{v}_h\right) - \left(\tilde{p}, \nabla \cdot \boldsymbol{v}_h\right) = \left(\rho^h \boldsymbol{g}, \boldsymbol{v}_h\right) + \left(\boldsymbol{t}_n, \boldsymbol{v}_h\right)_{\Gamma^{\boldsymbol{u}}_N} \end{aligned} \tag{30}$$

$$\begin{aligned} &\left(\rho^h c_p \tfrac{\partial T_h}{\partial t} + \rho^h c_p (\boldsymbol{u}_h + \tilde{\boldsymbol{u}}) \cdot \nabla T_h + 4\kappa_e \sigma_B \left(T_h + \tilde{T}\right)^4, w_h\right) \\ &\quad - \left(\tilde{T}, \rho^h c_p (\boldsymbol{u}_h + \tilde{\boldsymbol{u}}) \cdot \nabla w_h - \nabla^h \cdot (k \nabla w_h)\right) + \left(c_p \tfrac{\partial (\rho^h \tilde{T})}{\partial t}, w_h\right) \\ &\quad + (k \nabla T_h, \nabla w_h) = \left(Q + \tfrac{\mathrm{d}p^{\mathrm{th}}}{\mathrm{d}t} + \kappa_a G\left(I^d_{\lambda h}\right), w_h\right) + \left(q_n, w_h\right)_{\Gamma^T_N} \end{aligned} \tag{31}$$

$$\left(\mathcal{R}_M\left(I^d_{\lambda h} + \tilde{I}^d_{\lambda}, T_h + \tilde{T}\right), z_h\right) = 0 \tag{32}$$

for any test functions $\left(\boldsymbol{v}_h, q_h, w_h, z_h\right) \in \left(\boldsymbol{V}_{0,h} \times Q_{0,h} \times W_{0,h} \times Z_{0,h}\right)$, where:

$$\rho^h = \frac{p^{\mathrm{th}}}{R\left(T_h + \tilde{T}\right)} \tag{33}$$

is obtained applying the scale splitting to the state Equation (5). The symbol ∇^h in Equations (30) and (31) indicates that the integral is carried over the finite element interiors, and not over the edges, for example:

$$\left(\tilde{T}, \nabla^h \cdot (k \nabla w_h)\right) = \sum_K \left(\tilde{T}, \nabla \cdot (k \nabla w_h)\right)_K$$

where $(\cdot,\cdot)_K$ is the $L^2(K)$ inner product:

Remark 1. The radiation intensity subgrid scale in Equation (32) depends on the particular directional discretization used. As described in Section 2.2, our goal is to present a stabilization method independent of the directional discretization in the RTE. A complete discussion on the approximation of the radiation intensity subgrid scale when the DOM method is used can be found in Avila *et al.* (2011a, b). In turn, when, e.g. the P1 method is used, the resulting problem is elliptic and one can simply consider $\tilde{I}^d_\lambda = 0$. As this choice only affects the approximation of the RTE and not the coupling with the hydrodynamic problem we will consider $\tilde{I}^d_\lambda = 0$ in what follows. It is worth noting that the numerical results obtained using the DOM method presented in Section 6 were obtained using the approximation discussed in Avila *et al.* (2011a, b).

Remark 2. The temperature has been split into $T_h + \tilde{T}$ inside the radiative operator $\mathcal{R}_M$. If the temperature subgrid scale is neglected in Equation (32) it is convenient to neglect it also in the energy Equation (31). Otherwise energy will not be globally conserved, as it will be shown in Section 4.

Remark 3. It is known that the absorption coefficient k_a depends strongly on temperature, being correlated with the thermal radiation emission I_b and the radiation field I. It is very important to model these correlations, especially in combustion problems because temperature is highly fluctuating in space and time. When the temperature scale splitting is taken into account inside the radiative model, the absorption and emission coefficients k_a and k_e should be evaluated in terms of $T_h + \tilde{T}$ through Equations (9) and (10). The correlations between temperature and blackbody radiation I_b, and temperature and the radiative field I are modeled when computing k, G and I_b in terms of $T_h + \tilde{T}$. This is only done when introducing $T_h + \tilde{T}$ in the radiative model.

The nonlinear scale splitting of the convective terms (in the momentum and energy equations) permits to model turbulence without the use of any physical model. The behavior of this numerical method in the LES of thermally coupled turbulent flows at low Mach number is analyzed in Avila *et al.* (2014). The extension of the method to radiative flows leads to the (temperature) scale splitting of the nonlinear radiative terms. These terms are thought to model the physical subgrid behavior that cannot be captured by the mesh, and therefore to improve the obtained solutions of the equations. We have observed in numerical examples that the consideration of the temperature scale splitting $T_h + \tilde{T}$ in the energy and radiation equations increases the radiative heat flux from hot zones, being this effect peculiar of turbulence-radiation interaction models, as explained in Coelho (2007).

In order to give a closure to system Equations (29)-(33) we need to define how the subgrid scales $\tilde{u}$, $\tilde{p}$ and $\tilde{T}$ are computed. In the same way the finite element equations can be understood as the projection of the original equations onto the finite element spaces $\boldsymbol{Y}_h$, the equations for the subgrid scales are obtained by projecting the original equations onto their corresponding spaces $\tilde{\boldsymbol{Y}}$. The hydrodynamic subgrid-scale equations are written as:

$$\rho^h \nabla \cdot \tilde{\boldsymbol{u}} - \frac{\rho^h(\boldsymbol{u}_h + \tilde{\boldsymbol{u}})}{T_h + \tilde{T}} \cdot \nabla \tilde{T} = R_c + p_{ort} \tag{34}$$

$$\frac{\partial\left(\rho^h \tilde{\boldsymbol{u}}\right)}{\partial t}+\nabla\cdot\left(\rho^h(\boldsymbol{u_h}+\tilde{\boldsymbol{u}})\tilde{u}\right)-\nabla\cdot(2\mu\varepsilon'(\tilde{\boldsymbol{u}}))+\nabla\tilde{p}=\boldsymbol{R}_m+\boldsymbol{u}_{ort} \tag{35}$$

$$c_p\frac{\partial\left(\rho^h\tilde{T}\right)}{\partial t}+c_p\nabla\cdot\left(\rho^h(\boldsymbol{u}_h+\tilde{\boldsymbol{u}})\tilde{T}\right)-\nabla\cdot\left(k\nabla\tilde{T}\right)=R_e+T_{ort} \tag{36}$$

where p_{ort}, $\boldsymbol{u}_{ort}$ and T_{ort} are functions L_2-orthogonal to the subgrid-scale space, responsible to guarantee that the subgrid-scale equations belong to the subgrid-scale spaces. The residuals of mass, momentum and energy equations are, respectively:

$$R_c=-\frac{\partial\rho^h}{\partial t}-\rho^h\nabla\cdot\boldsymbol{u}_h+\frac{\rho^h(\boldsymbol{u}_h+\tilde{\boldsymbol{u}})}{T_h+\tilde{T}}\cdot\nabla T_h \tag{37}$$

$$\boldsymbol{R}_m=\rho^h\boldsymbol{g}-\rho^h\frac{\partial\boldsymbol{u}_h}{\partial t}-\rho^h(\boldsymbol{u}_h+\tilde{\boldsymbol{u}})\cdot\nabla\boldsymbol{u}_h+\nabla\cdot(2\mu\varepsilon'(\boldsymbol{u}_h))-\nabla p_h \tag{38}$$

$$R_e=Q+\frac{\mathrm{d}p^{\mathrm{th}}}{\mathrm{d}t}-\rho^h c_p\frac{\partial T_h}{\partial t}-\rho^h c_p(\boldsymbol{u}_h+\tilde{\boldsymbol{u}})\cdot\nabla T_h+\nabla\cdot(k\nabla T_h)+\kappa G-4\kappa_e\sigma_B\left(T_h+\tilde{T}\right)^4 \tag{39}$$

3.1 Approximation of the subgrid scales

We will approximate the subgrid-scale problem replacing the (spatial) differential operators of mass, momentum and energy equations by the algebraic operators τ_c^{-1}, τ_m^{-1} and τ_e^{-1}, respectively. The approximation to the subgrid-scale Equations (34)-(36) within each element of the finite element partition reads:

$$\frac{1}{\tau_c}\tilde{p}=R_c+p_{ort}=R_c' \tag{40}$$

$$\frac{\partial\left(\rho^h\tilde{\boldsymbol{u}}\right)}{\partial t}+\frac{1}{\tau_m}\tilde{\boldsymbol{u}}=\boldsymbol{R}_m+u_{ort}=\boldsymbol{R}_m' \tag{41}$$

$$c_p\frac{\partial\left(\rho^h\tilde{T}\right)}{\partial t}+\frac{1}{\tau_e}\tilde{T}=R_e+T_{ort}=R_e' \tag{42}$$

The stabilization parameters τ_c, τ_m and τ_e are defined as:

$$\tau_c=\frac{h^2}{c_1\rho^h\tau_m}=\frac{\mu}{\rho^h}+\frac{c_2}{c_1}\left|\boldsymbol{u}_h+\tilde{\boldsymbol{u}}\right|h \tag{43}$$

$$\tau_m = \left(c_1 \frac{\mu}{h^2} + c_2 \frac{\rho^h | \boldsymbol{u}_h + \tilde{\boldsymbol{u}} |}{h} \right)^{-1} \tag{44}$$

$$\tau_e = \left(c_1 \frac{k}{h^2} + c_2 \frac{\rho^h c_p | \boldsymbol{u}_h + \tilde{\boldsymbol{u}} |}{h} \right)^{-1} \tag{45}$$

where h is the element size and c_1 and c_2 are algorithmic constants whose values for linear elements are $c_1 = 4$ and $c_2 = 2$ in the numerical examples. It is important to remark that Equations (41) and (42) are nonlinear equations. These subgrid-scale equations are solved at each numerical integration point of the mesh. The functions p_{ort}, $\boldsymbol{u}_{ort}$ and T_{ort} depend on the choice of the subgrid-scale space $\tilde{\boldsymbol{Y}}$. The easiest choice is to consider the space of subgrid scales as that of the residuals, that amounts to take p_{ort}, u_{ort} and T_{ort} equal zero. Another possibility consists in taking precisely $\tilde{\boldsymbol{Y}} = \boldsymbol{Y} \cap \boldsymbol{Y}_h^{\perp}$, the orthogonality understood with respect to the inner product $(u, \rho^h v)$. From this definition, the functions p_{ort}, $\boldsymbol{u}_{ort}$ and T_{ort} are calculated from the equalities $(\rho^h \tilde{\boldsymbol{u}}, \boldsymbol{v}_h) = 0$, $(\rho^h \tilde{T}, \boldsymbol{w}_h) = 0$ and $(\rho^h \tilde{p}, \boldsymbol{q}_h) = 0 \ \forall (\boldsymbol{v}_h, w_h, q_h) \in (\boldsymbol{V}_h \times W_h \times Q_h)$. A deeper insight about the present subgrid-scale model can be found in Avila *et al.* (2011a, b, 2014), where also some linearization schemes are presented:

Remark 4. The spatial-differential operator in the subgrid-scale Equation (36) has been approximated to obtain Equation (42). Note however, that $\tilde{T}$ still appears in the right hand side of Equation (42) in the nonlinear reactive term $\kappa_e \sigma_B (T_h + \tilde{T})^4$. In the case of a linear convection-diffusion-reaction equation the reactive term is kept on the left hand side and a stabilization parameter of the form:

$$\tau_e = \left(c_1 \frac{k}{h^2} + c_2 \frac{\rho^h c_p | \boldsymbol{u}_h + \tilde{\boldsymbol{u}} |}{h} + c_3 \kappa_e \right)^{-1}$$

is considered. Following the same approach we propose here in the limit case of linear equation we obtain the same result with $c_3 = 1$, which turns out to be the value recommended in (Codina, 1998).

4. Global energy conservation

The aim of this section is to obtain a global conservation of energy statement similar to those holding for the continuous problem, but for the problem semi-discretized in space. It has been shown in Avila *et al.* (2011a, b) that global conservation statements for mass, momentum and energy without radiative terms hold when equal interpolation is used for all variables. We shall see that the total energy will be globally conserved only if the radiative model $\mathcal{R}_M$ conserves radiation energy.

When the radiation transfer Equation (4) is integrated over all solid angle directions, and over all the spectral domain $\lambda \in \mathbb{R}^+$, the zeroth moment radiative equation is obtained:

$$\nabla \cdot \boldsymbol{q}_r - \kappa_a G = 4 \kappa_e \sigma_B T^4$$

This equation is satisfied by most radiative models that can be understood as angular discretization, as DOM and P_1. After integration of this equation over all the spatial

domain Ω, the following radiation conservation statement for the continuous problem is obtained:

$$\int_{\Omega}\left(4\kappa_e\sigma_B T^4-\kappa_a G\right)d\Omega=\int_{\partial\Omega}\boldsymbol{q}_r\cdot\boldsymbol{n}\,\mathrm{d}\Gamma \tag{46}$$

When the discrete counterpart of this conservation statement is satisfied by the discrete approximation of radiative models $\mathcal{R}_M$ Equation (32), it is said that the radiation model conserves radiation energy. This is the case of the finite element approximation of the DOM and the P_1 method, which read:

$$\int_{\Omega}\left(4\kappa_e\sigma_B\left(T_h+\tilde{T}\right)^4-\kappa_a G\right)d\Omega=\int_{\partial\Omega}\boldsymbol{q}_r\cdot\boldsymbol{n}\,\mathrm{d}\Gamma \tag{47}$$

Let us consider the finite element space for the temperature equation without Dirichlet boundary conditions, and an augmented problem that also contains the fluxes at the Dirichlet boundaries as unknowns (Hughes *et al.*, 2000). When using equal interpolation spaces for the temperature and pressure equations ($W_h=Q_h$), it can be shown that taking the test function $w_h=1$ in (the augmented problem corresponding to) the finite element energy Equation (31), and replacing Equation (47) we get the relation:

$$\int_{\Omega}c_p\frac{\partial}{\partial t}\left(\rho^h\left(T_h+\tilde{T}\right)\right)\mathrm{d}\Omega=\int_{\Omega}\left(Q+\frac{\mathrm{d}p^{\mathrm{th}}}{\mathrm{d}t}\right)\mathrm{d}\Omega-\int_{\partial\Omega}\left(q_n+\boldsymbol{n}\cdot\left(\boldsymbol{q}_r+\boldsymbol{u}_h\rho^h c_p T_h\right)\right)\mathrm{d}\Gamma \tag{48}$$

which is the discrete counterpart of energy conservation Equation (3) integrated over domain Ω. Therefore, Equation (48) implies energy conservation. For ideal gases the internal energy per unit mass is $e=c_v T$, where $c_v\equiv c_p/\gamma$. According to that, we define at the discrete level the discrete internal energy per unit volume as $\rho^h e^h=\rho^h c_v(T_h+\tilde{T})$. Replacing this definition in Equation (48), after some operations (see Avila *et al.* 2011a, b), we arrive to the first law of thermodynamics for open systems in terms of the internal energy:

$$\int_{\Omega}\frac{\partial\left(\rho^h e_h\right)}{\partial t}\mathrm{d}\Omega=\int_{\Omega}Q\mathrm{d}\Omega+\int_{\partial\Omega}\left(q_n+q_{rn}-\boldsymbol{n}\cdot\boldsymbol{u}_h\left(\rho^h e^h+p^{\mathrm{th}}\right)\right)\mathrm{d}\Gamma \tag{49}$$

where $q_{rn}=\boldsymbol{q}_r\cdot\boldsymbol{n}$ is the radiative heat flux leaving the domain. This equation indicates that the change in internal energy of the system is equal to the heat power added to the system plus the work done over the system $\left(-\int_{\partial\Omega}\boldsymbol{n}\cdot\boldsymbol{u}_h p^{\mathrm{th}}\mathrm{d}\Gamma=-p^{\mathrm{th}}\int_{\Omega}\nabla\cdot\boldsymbol{u}_h\mathrm{d}\Omega\right)$ plus the boundary fluxes of heat and internal energy, q_n+q_{rn} and $\boldsymbol{n}\cdot\boldsymbol{u}_h\rho^h e^h$.

To satisfy the energy conservation statement Equation (48), and therefore Equation (49), the discrete radiative model Equation (32) must conserve the discrete radiation energy (statement Equation (47)). The discrete radiation equation must depend on the temperature scale splitting $T_h+\tilde{T}$ to be consistent with the temperature scale splitting in the energy equation, to achieve the energy conservation statement Equation (47). If this splitting is ignored in the radiative model Equation (32) ($(\mathcal{R}_M(I^d_{\lambda h}, T_h), z_h)=0$), then the radiative term in the energy Equation (31) should be introduced in the form $4\kappa_e\sigma_B T_h^4$ to have a global energy conservative scheme.

5. Linearization strategy of coupling terms between radiation and temperature equations

The coupling between radiation and energy equations is extremely nonlinear, and careful linearization schemes should be used to achieve a converged solution of the problem. In this section we discuss the linearization of the terms involved in radiation. Linearization schemes of mass, momentum and energy equations without considering radiative coupling are explained in Avila *et al.* (2011a, b).

5.1 Linearization of radiative terms in the finite element equation

We will focus on how to linearize the energy Equation (31); the radiative Equation (32) is supposed to be solved in segregated form. The subgrid scales are supposed to be given as we need to solve the finite element problem Equation (31). The linearization of the radiative term $4\kappa_e\sigma_B(T_h+\tilde{T})^4$ in the energy equation using a Newton-Rapshon scheme is always convergent, because this term never changes its convexity (second derivative sign respect to T_h remains unchanged). If the temperature T_h is known at iteration k, the nonlinear term is linearized at iteration k+1 in terms of T_h^{k+1}, using a Newton-Raphson scheme as:

$$4\kappa_e\sigma_B\left(T_h^{k+1}+\tilde{T}\right)^4 \approx 4\kappa_e\sigma_B\left(T_h^{k}+\tilde{T}\right)^3\left(4T_h^{k+1}-3T_h^{k}+\tilde{T}\right) \tag{50}$$

Other linearization strategies were implemented, like the fixed-point iteration:

$$4\kappa_e\sigma_B\left(T_h^{k+1}+\tilde{T}\right)^4 \approx 4\kappa_e\sigma_B\left(T_h^{k}+\tilde{T}\right)^3\left(T_h^{k+1}+\tilde{T}\right)$$

or the following:

$$4\kappa_e\sigma_B\left(T_h^{k+1}+\tilde{T}\right)^4 \approx 4\kappa_e\sigma_B\left(T_h^{k}+\tilde{T}\right)^3\left(2T_h^{k+1}-T_h^{k}+\tilde{T}\right)$$

These iterations schemes diverged in many examples. The Newton-Raphson scheme Equation (50), besides being unconditionally convergent, converged always faster than the other linearization schemes.

We have solved the radiation Equation (32) segregated from the temperature Equation (31). The coupling between radiation and temperature equations has been found to converge much faster when applying an over-relaxation to temperature.

5.2 Linearization of radiative terms in the subgrid-scale equation

The subgrid-scale equations form a nonlinear system of equations that must be linearized. Linearization schemes for the subgrid-scale equations without considering radiation coupling are detailed in Avila *et al.* (2011a, b), where it was shown that the Newton-Raphson scheme applied to the monolithically coupled system of equations was the most efficient one. Radiative transfer introduces the nonlinear term $4\kappa_e\sigma_B(T_h+\tilde{T})^4$ in the subgrid-scale energy Equation (36). The Newton-Raphson scheme for the linearization of this radiative term inside the subgrid-scale energy Equation (36) is (again) unconditionally convergent, because the function does not change its convexity. The finite element unknowns are assumed to be given as we need to solve the subgrid-scale problem. If the temperature subgrid scale is known at iteration k, the linearization of the nonlinear reactive term with respect to $\tilde{T}^{k+1}$ at iteration $k+1$ is:

$$4\kappa_e\sigma_B\left(T_h+\tilde{T}^{k+1}\right)^4 \approx 4\kappa_e\sigma_B\left(T_h+\tilde{T}^{k}\right)^3\left(T_h+4\tilde{T}^{k+1}-3\tilde{T}^{k}\right) \tag{51}$$

We obtained satisfactory and fast convergent results using this scheme.

5.3 Linearization of the coupled energy boundary condition

When we want to impose an amount of conductive plus radiative heat flux through the boundaries, $q_n + q_{rn} = \mathcal{H}$, we need to apply the nonlinear boundary condition Equation (19) to the energy Equation (31). This condition couples temperature and radiation intensity on the boundary, affecting significantly the solution for optically thin problems, in which $k_a L < 1$, where L is a characteristic length of the problem. We have found in the numerical experiments that a proper linearization of this boundary condition needs to be applied to achieve convergence. The most efficient method was to apply a Newton-Raphson scheme. Although it is always convergent, the solution converged extremely slowly when solving optically thin problems. When applying simpler linearization schemes the solution did not converge.

Assuming a known temperature at iteration k, boundary condition Equation (19) is linearized to approximate temperature at iteration k+1 as:

$$-\boldsymbol{n}\cdot k\nabla T_h^{k+1} - \varepsilon\sigma_B\left(T_h^k\right)^3\left(4T_h^{k+1} - 3T_h^k\right) = \mathcal{H} - (1-r)H \tag{52}$$

The resulting linearized boundary condition is of Robin type.

6. An application example: fire in a 3D room with an open door

This test example is a fire compartment similar to that considered in Avila *et al.* (2011a, b), but now simulating the effect of radiative heat transfer. In order to increase radiative heat transfer effects, the power of the heat source that models the fire has been increased.

The problem domain is $\Omega = [0, L] \times [0, L] \times [0, H]$ where $L = 2.8$ m and $H = 2.18$ m. The compartment has an open door on the side wall of the room ($x = L$) whose dimension is 0.7×1.853 m^2. A scheme of the problem domain is shown in Figure 1. The fire is modeled by an uniform heat source of 30 kW, located at the center of the room just over the floor, with dimensions $0.84 \times 0.84 \times 0.218$ m^3. Adiabatic boundary conditions are imposed on all the walls. Non slip boundary conditions for velocity are

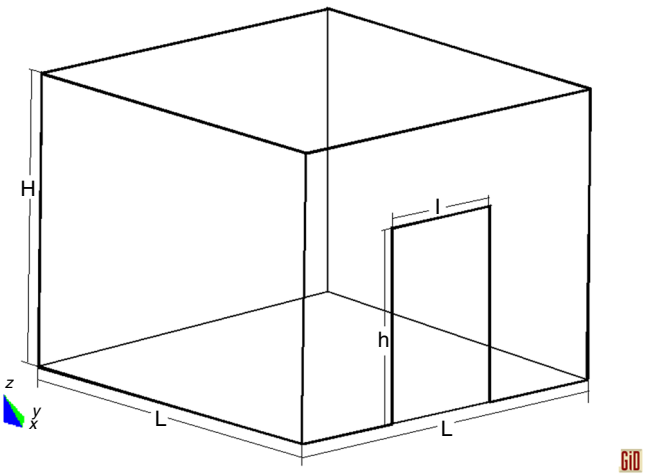

Figure 1.
Problem domain of the room with an open door

imposed on all the boundaries except the door, where atmospheric boundary condition is imposed, that is, a traction $t_n = (-\rho|g|z, 0, 0)$. As the flow is open $\left(\left(\Gamma_N^u \neq \emptyset\right)\right)$, the thermodynamic pressure is set constant in time to $p^{\text{th}} = 101325$ Pa. The initial temperature and velocity values are $T_0 = 300$ K and $\boldsymbol{u}_0 = \mathbf{0}$ over all domain Ω. Furthermore, the viscosity is $\mu = 0.0094$ kg/m s and $\text{Pr} = 0.71$. The gravity is set to $\boldsymbol{g} = (0, 0, -9.8)$ m/s^{-2}. The medium is treated as a gray body, with homogeneous absorption and emissive coefficientes $k_a = k_e = 10$ m^{-1}, and a zero scattering coefficient $\sigma_s = 0$.

The radiative field was obtained using both the spherical harmonics P_1, and the DOM approximation to the radiative transport equation. For the DOM discretization we used the $S10$ (Lathrop, 1966) set of ordinates and weights for DOM, consisting in 120 ordinates.

The compartment was meshed using a grid of $40 \times 40 \times 40$ uniform trilinear elements Q_1. We solved the problem using finite-difference time integration schemes, with uniform step size of $\delta t = 1.0$ s. We compared the obtained solutions with three different stabilization methods, namely, the classical SUPG method, and the dynamical and nonlinear subgrid-scale method presented in this paper with and without temperature scale splitting of the radiative term, $4k\sigma_B T^4$. We call this method DSS in the following. When temperature scale splitting is (not) considered in the energy equation, then it is also (not) considered as radiative source in the radiation equation. In the present example the subgrid-scale space is considered as that of the residuals, and p_{ort}, $\boldsymbol{u}_{ort}$ and T_{ort} equal zero in Equations (40)-(42). The obtained results are compared against a reference solution obtained using the SUPG method over a fine mesh of $80 \times 80 \times 80$ uniform elements, and a time step size of $\delta t = 0.5$ s, using the P_1 method and the DOM. The computation is advanced until $t_{\text{end}} = 180.0$ s using the second-order time integration scheme BDF2. The tolerance for the nonlinear iterations was set to 5.10^{-4} in the relative norm of the difference between two iterates.

In Figures 2-4 the temperature and vertical velocity distributions along the x, y and z directions using the DSS and SUPG methods at $t = t_{\text{end}}$ are shown for the P_1 method. The same results are shown when using the DOM in Figures 5-7 using the DOM. TheDSS method is labeled as FullSplitDSS when the temperature subgrid scale is kept in all terms, and it is labeled as DSSwTh4 when the temperature subgrid scale is not taken into account in the radiative term. In all those figures the greater similarity of the results with the reference solution when using the DSS method against SUPG method is

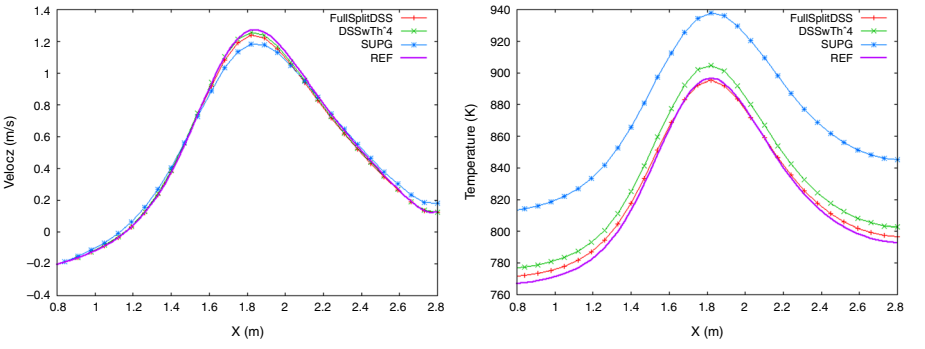

Figure 2. Temperature and vertical velocity distributions along the x direction using the P_1 method, $y = 1.4$ m, $z = 0.763$ m

clearly observed, in spite of the fact that the reference solution was obtained using the SUPG method on a finer mesh. The same observation was done in Avila *et al.* (2011a, b) for the problem without radiation. It is observed that performing the temperature scale splitting in the radiative term has the effect of decreasing the obtained temperature, closer to the reference solution. The effect of the temperature splitting is more noticeable in the temperature solution; the vertical velocity is less affected, and it is difficult to conclude if there exists an improvement.

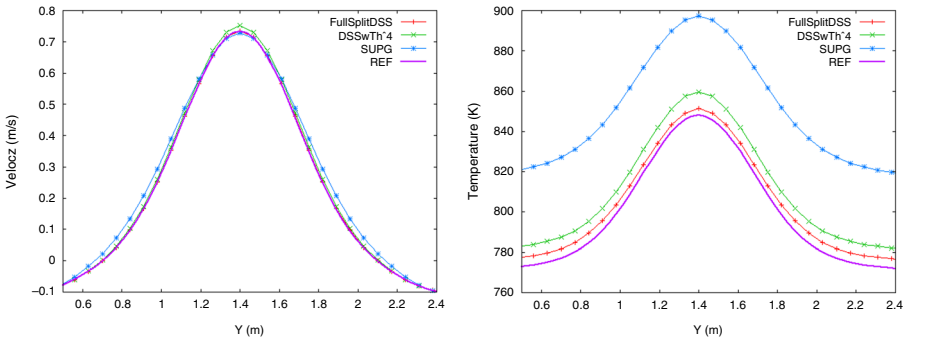

Figure 3.
Temperature and vertical velocity distributions along the y direction using the P_1 method, $x = 1.54$ m, $z = 0.763$ m

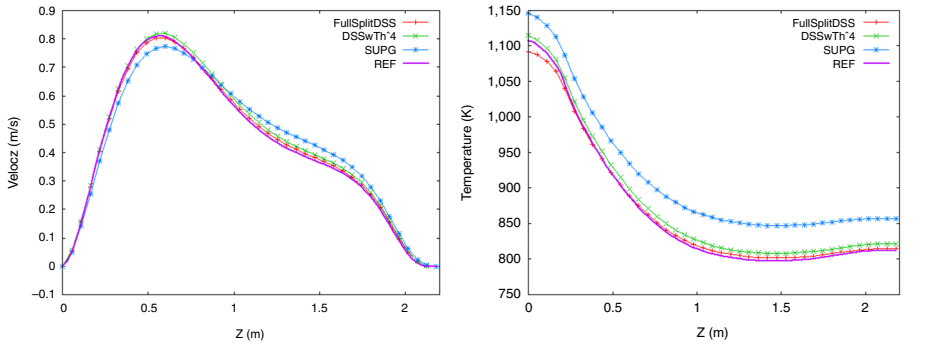

Figure 4.
Temperature and vertical velocity distributions along the z direction using the P_1 method, $x = 1.54$ m, $y = 1.4$ m

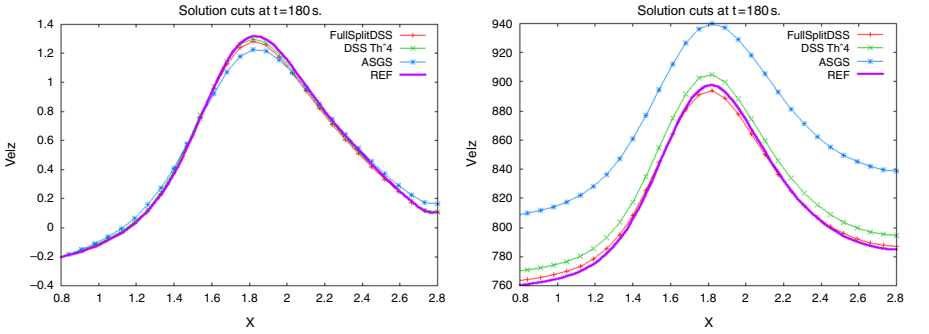

Figure 5.
Temperature and vertical velocity distributions along the x direction using the DOM, $y = 1.4$ m, $z = 0.763$ m

The time evolution of temperature and vertical velocity (along the z direction) at points of coordinates (1.55, 1.4, 0.55), (1.3 1.3, 0.2) and (1.4, 1.4, 1.0) (in meters) are compared in Figures 8-10 for the P_1 method, and in Figures 11-13 for the DOM.It is observed again that when using the SUPG method the solution differs much more from the reference solution than when using the DSS method. It is difficult to observe the difference in the solutions when splitting or not the temperature in the radiative term, and it is even

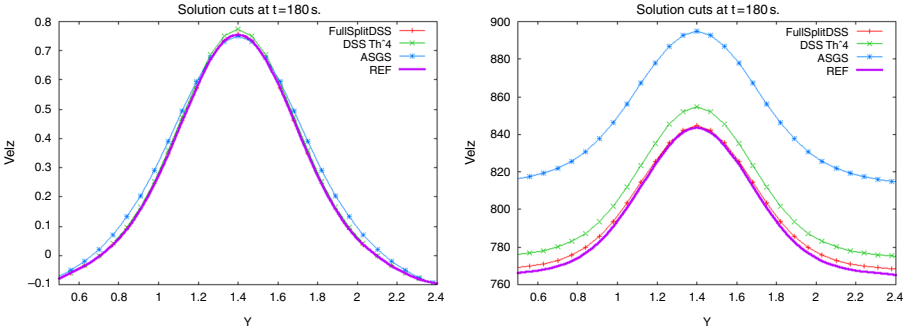

Figure 6.
Temperature and vertical velocity distributions along the y direction using the DOM, $x = 1.54$ m, $z = 0.763$ m

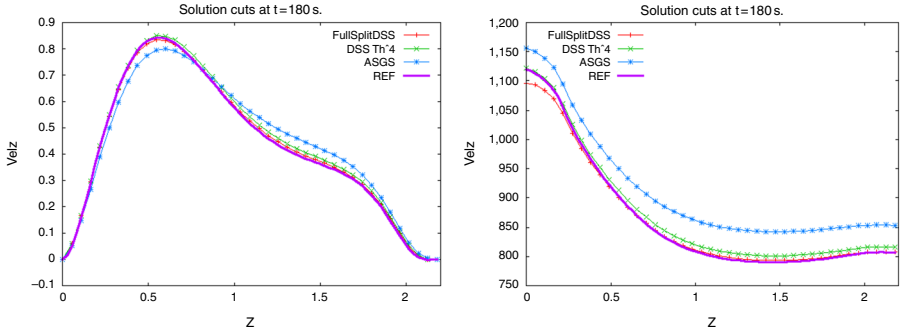

Figure 7.
Temperature and vertical velocity distributions along the z direction using the DOM, $x = 1.54$ m, $y = 1.4$ m

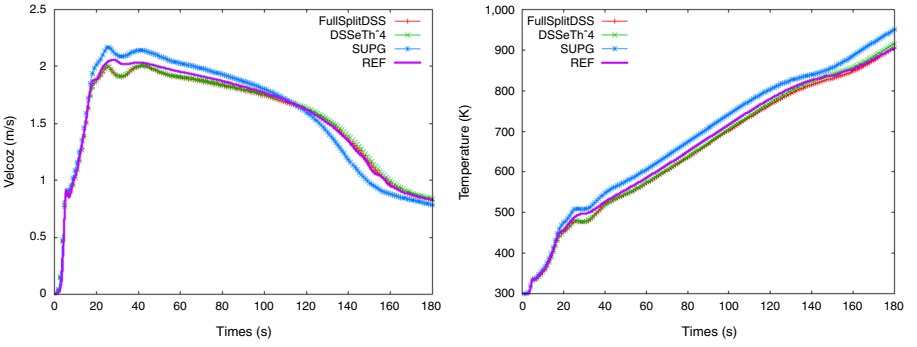

Figure 8.
Time evolution of temperature and vertical velocity (i.e. u_z) at point (1.55, 1.4, 0.55) m using P_1 method

more difficult to confirm if there exist any improvement. However, observing temperature cuts at time t_{end} it is seen that there exists such an improvement in temperature field.

In Figure 14 the obtained temperature distribution along the x and y directions are compared when using the DOM and the P_1 methods. The small difference in the solution indicates that the P_1 method gives reasonable good solutions. This is due to

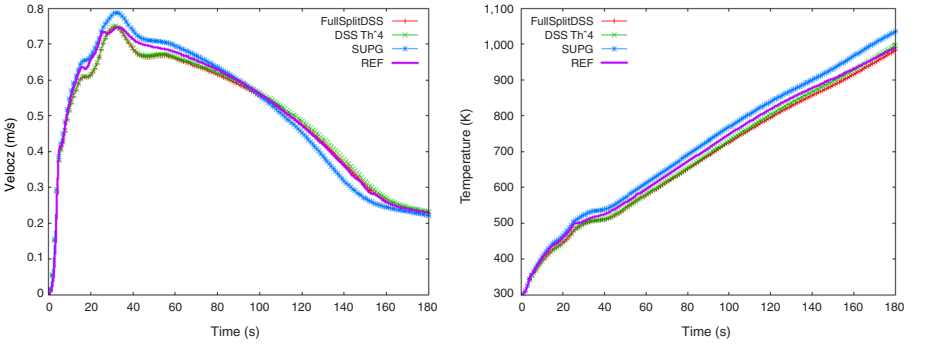

Figure 9.
Time evolution of temperature and vertical velocity (i.e. u_z) at point (1.3, 1.3, 0.2) m using P_1 method

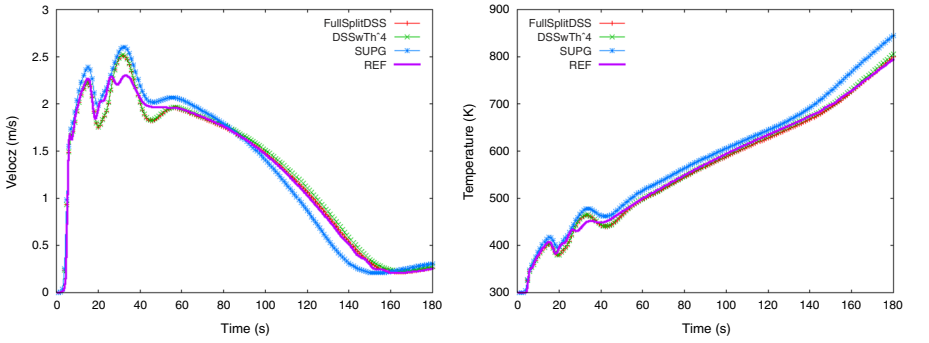

Figure 10.
Time evolution of temperature and vertical velocity (i.e. u_z) at point (1.4, 1.4, 1.0) m using P_1 method

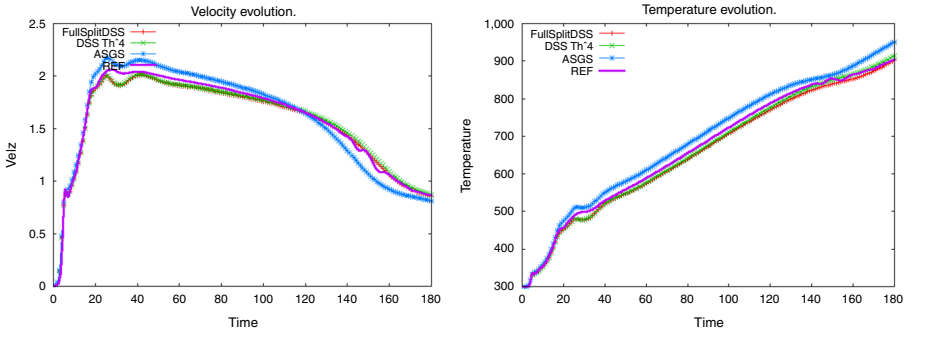

Figure 11.
Time evolution of temperature and vertical velocity (i.e. u_z) at point (1.55, 1.4, 0.55) m using the DOM

the fact that the linearly anisotropic angular distribution of radiation intensity assumed by the P_1 method is a good approximation, since we are in an optically thick case ($\tau \approx 25$).

In Figure 15 the distribution of the temperature subgrid scale over the plane $y = L/2$ when $t = t_{end}$ is shown. It is seen that the maximum subgrid-scale values are located over the source term position, contributing to a raise of radiation source when adding the temperature subgrid scale. We would like to mention that a spatial temperature

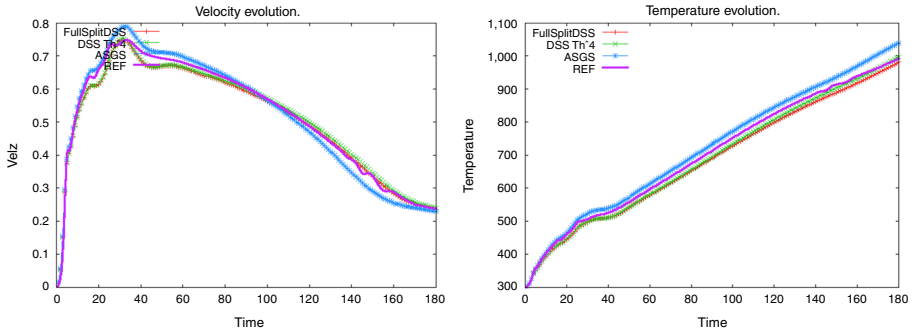

Figure 12. Time evolution of temperature and vertical velocity (i.e. u_z) at point (1.3, 1.3, 0.2) m using the DOM

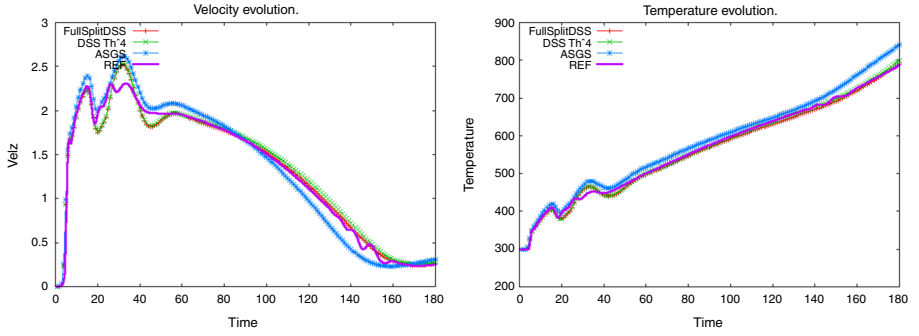

Figure 13. Time evolution of temperature and vertical velocity (i.e. u_z) at point (1.4, 1.4, 1.0) m using the DOM

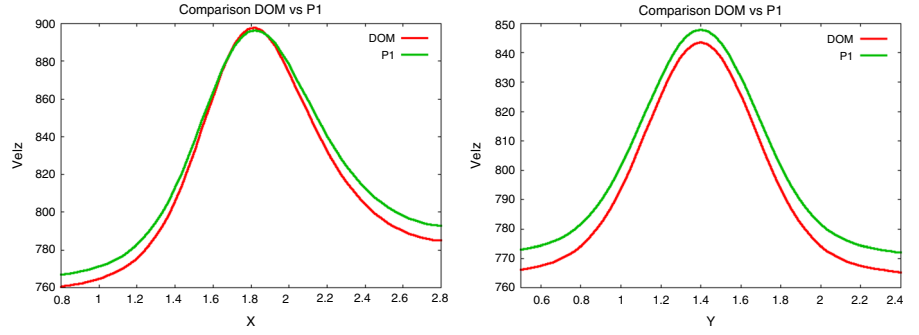

Figure 14. Temperature distribution along x and y direction using the P1 method and the DOM

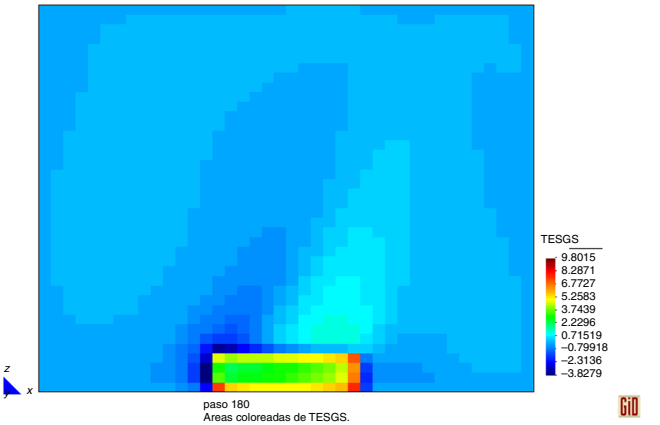

Figure 15.
Temperature subgrid-scale distribution on the plane $y = L/2$)

subgrid-scale distribution over the source with mean value zero, and zero skewness, would contribute to a positive raise of the radiative source. In Figure 16 the temperature distribution over the plane $y = L/2$ at time $t = t_{\text{end}}$ when considering and not considering the temperature subgrid scale in the radiative term of the energy equation are shown. The effect of considering the full-scale splitting is a temperature decrease, a similar effect of radiation-turbulence interaction models. Figure 16 shows the radiative heat distribution over the plane $y = L/2$ at time $t = t_{\text{end}}$ when considering and not considering the temperature subgrid scale in the radiative term of the energy equation. It is seen that the radiative heat flux decreases when considering the temperature splitting, which is due to the decrease of temperature over the fire.

The effect of considering temperature scale splitting in the radiative term $4\kappa\sigma_B(T_h + \tilde{T})^4$ enhances the obtained results, increasing the radiative heat flux from hot zones. This is the expected turbulent effect of modeling a subgrid temperature. We believe that the difference in the results when considering the temperature subgrid scale in the radiative term will be more noticeable in turbulent flames, with combustion models. We expect that for turbulent flows the effect of modeling the emitting and absorbing radiation effects as $4\kappa_e(T)\sigma_B(T_h + \tilde{T})^4$, in a purely numerical form, will model the turbulent radiation interaction enhancing the obtained solution.

6.1 Performance of the methods

The total number of nonlinear iterations needed to solve the problem (i.e. the sum of the nonlinear iterations performed in all time steps) and the total CPU time are indicated in Table I when using the P_1 method. The CPU time spent when using the DOM is much higher for the radiation problem, but it is similar for the low Mach number problem. The CPU time spent for the assembly of the low Mach equations (which includes numerical integration and solution of the subgrid-scale problem, i.e. operations involving a loop over integration points) and the CPU time spent in the (linear) solver procedures are also indicated. The CPU time spent solving the radiation equation is also indicated.

The total number of nonlinear iterations for the low Mach equations is 5 percent lower using the DSS method respect to the SUPG method. However, the use of the

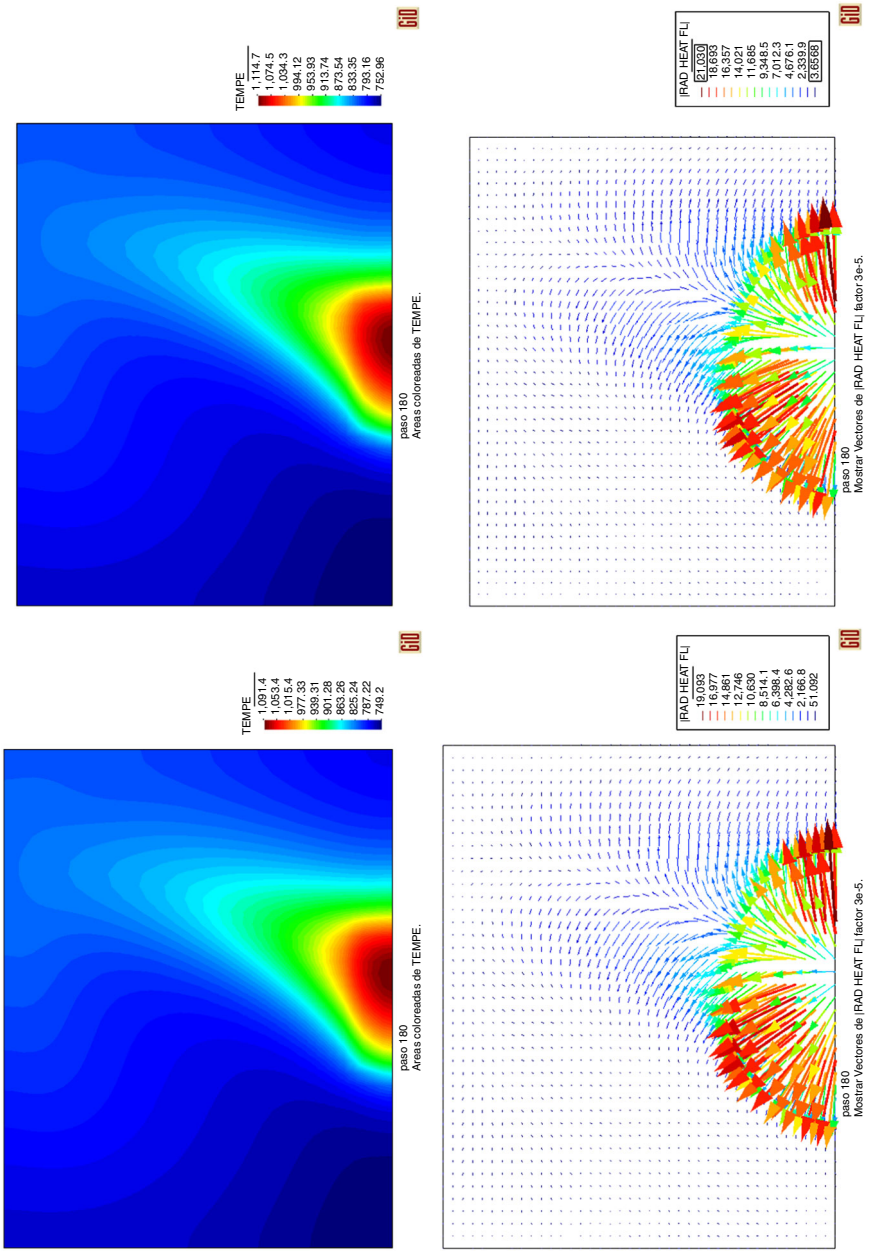

Figure 16.
Temperature distribution and radiative heat flux distribution over plane $y = L/2$ when splitting radiative term as $4\kappa\sigma_B\left(T_h+\tilde{T}\right)^4$ (left) and not splitting $4\kappa\sigma_B T_h^4$ (right)

DSS method increases the CPU time of assembly operations per iteration, and therefore the total CPU time is 6.5 percent higher using DSS method respect to SUPG, but the obtained solution is much better. The same behavior was observed in the same problem in Avila *et al.* (2011a, b), without radiation, using a smaller fire source and the same mesh with the same time step. The DSS method is observed to be very competitive. The CPU time spent solving the radiation equations does not differ more than 1 percent using the different methods in low Mach number equations. The CPU time of DSS method does not change when taking into account the temperature splitting in the radiative term. The CPU solver time is a little lower using the SUPG method, that is, the system is a little better conditioned. This is due to the spatial discontinuities of the subgrid scales that worsens the matrix condition. This small extra CPU time when using DSS method occurs at expenses of obtaining a much better solution.

7. Conclusions

A finite element approximation of the low Mach number equations coupled with a radiative heat transfer model based on a splitting of the unknowns into finite element and unresolvable components has been developed. The main ingredients of the formulation are:

- to consider time dependent subgrid scales; and
- to keep the subgrid-scale components in all the nonlinear terms.

The effect of considering time dependent subgrid scales is well known (Codina *et al.*, 2007) and our experience with the low Mach number equations (Avila *et al.*, 2011a, b, 2014) confirms the properties known for incompressible flows. The effect of considering the splitting of the unknowns in all the terms leads to a more accurate solution than classical stabilization methods and provides global mass, momentum and energy conservation when using equal interpolation spaces for the velocity, pressure and temperature equations. An improvement in the quality of the solution is obtained when considering the spliting of the radiation terms in the temperature equation.

We would like to stress, once again, that we keep the splitting of the unknowns in all terms also in the subscale equations, and we have numerically verified that this makes a difference in the accuracy of the scheme.

This nonlinear and transient treatment of the subgrid scales has a computational cost, both in memory requirements and in CPU time. Nevertheless, the extra amount of memory needed only grows linearly with the number of nodes and will be usually dominated by the memory needed to solve the linear system and, as we have observed, the increase of CPU time in the DSS is very small.

The formulation intrinsically contains cross- and Reynolds-stress terms, and TRI terms that try to model the unsolved eddies and subgrid interaction between

Table I.
Comparison of the total number of iterations and the required CPU time for the different methods

	No. of iters	Total CPU(s)	CPU LM(s)	CPU Rad(s)	CPU assem LM(s)	CPU solv LM(s)
SUPG	3,579	82,563	66,182	16,341	24,159	42,023
DSSwTh4	3,438	88,105	71,896	16,144	28,359	43,537
DSSFULL	3,406	88,103	71,985	16,054	28,549	43,436

radiation and temperature, presenting an open door to turbulence modeling. The present method remains unchanged irrespective of whether laminar, transitional and turbulent situations are present.

We have emphasized the advantages of the temperature splitting $(T_h + \tilde{T})$ inside the radiative model and the radiative terms in the energy equation. When performing this splitting more accurate solutions were found in the numerical examples.

References

An, W., Ruan, L., Qi, H. and Liu, L. (2005), "Finite element method for radiative heat transfer in absorbing and anisotropic scattering media", *Journal of Quantitative Spectroscopy & Radiative Transfer*, Vol. 96 No. 3, pp. 409-422.

Avila, M., Codina, R. and Principe, J. (2011a), "Spatial approximation of the radiation transport equation using a subgrid-scale finite element method", *Computer Methods in Applied Mechanics and Engineering*, Vol. 200 No. 5, pp. 425-438.

Avila, M., Codina, R. and Principe, J. (2014), "Large eddy simulation of low Mach number ows using dynamic and orthogonal subgrid scales", *Computers & Fluids*, Vol. 99, pp. 44-66.

Avila, M., Principe, J. and Codina, R. (2011b), "A finite element dynamical nonlinear subscale approximation for the low Mach number equations", *Journal of Computational Physics*, Vol. 230 No. 22, pp. 7988-8009.

Codina, R. (1998), "Comparison of some finite element methods for solving the diffusion-convectionreaction equations", *Computer Methods in Applied Mechanics and Engineering*, Vol. 156 No. 1, pp. 185-210.

Codina, R., Principe, J., Guasch, O. and Badia, S. (2007), "Time dependent subscales in the stabilized finite element approximation of incompressible flow problems", *Computer Methods in Applied Mechanics and Engineering*, Vol. 196 No. 21, pp. 2413-2430.

Coelho, P. (2007), "Numerical simulation of the interaction between turbulence and radiation in reactive ows", *Progress in Energy and Combustion Science*, Vol. 33 No. 4, pp. 311-383.

Davison, B. (1958), *Neutron Transport Theory*, Oxford University Press, London.

Dubroca, B., Seaid, M. and Teleaga, I. (2007), "A consistent approach for the coupling of radiation and hydrodynamics at low Mach number", *Journal of Computational Physics*, Vol. 225 No. 1, pp. 1039-1065.

Hughes, T. (1995), "Multiscale phenomena: green's function, the Dirichlet-to-Neumann formulation, subgrid scale models, bubbles and the origins of stabilized formulations", *Computer Methods in Applied Mechanics and Engineering*, Vol. 127 No. 1, pp. 387-401.

Hughes, T., Emgel, G., Mazzei, L. and Larson, M. (2000), "The continuous Galerkin method is locally conservative", *Journal of Computational Physics*, Vol. 163 No. 2, pp. 467-488.

Hun-Kang, S. and Song, T.-H. (2008), "Finite element formulation of the first- and second- order discrete ordinates equations for radiative heat transfer calculation in three dimensional participating media", *Journal of Quantitative Spectroscopy & Radiative Transfer*, Vol. 109 No. 11, pp. 2094-2107.

Lathrop, K. (1966), "Use of discrete-ordinate methods for solution of photon transport problems", *Nuclear Science and Engineering*, Vol. 24 No. 4, pp. 381-388.

Modest, M. (1976), "Photon-gas formulation of the differential approximation in radiative transfer", *Letters in Heat and Mass Transfer*, Vol. 3 No. 2, pp. 111-116.

Modest, M. (2003), *Radiative Heat Transfer*, Academic Press, NewYork, NY.

Razzaque, M., Klein, D. and Howell, J. (1983), "Finite element solution of radiative heat transfer in two dimensional rectangular enclosure with gray participating media using finite elements", *J Heat Transfer*, Vol. 105 No. 4, pp. 933-936.

Truelove, J. (1987), "Discrete-ordinate solution of the radiation transport equation", *ASME Journal of Heat Transfer*, Vol. 109 No. 4, pp. 1048-1051.

Zeytounian, R.K. (2010), "Topics in hyposonic flow theory", Lect. Notes Phys. 672, Springer, Berlin Heidelberg.

Zhao, J. and Liu, L. (2007), "Second order radiative transfer equation and its properties of numerical solution using the finite element method", *Numerical Heat Transfer, Part B*, Vol. 51 No. 4, pp. 391-409.

Corresponding author
Dr R. Codina can be contacted at: ramon.codina@upc.edu